Journal of Colloid and Interface Science **228,** 344–358 (2000)
doi:10.1006/jcis.2000.6832, available online at http://www.idealibrary.com on IDEAL®

Removal of Solid Organic Films from Rotating Disks Using Emulsion Cleaners

J. A. Kabin,* S. T. Withers,* C. S. Grant,* R. G. Carbonell,*,[1] and A. E. Sáez†

*Department of Chemical Engineering, North Carolina State University, Box 7905, Raleigh, North Carolina 27695-7905; and †Department of Chemical and Environmental Engineering, University of Arizona, Tucson, Arizona 85721

Received June 30, 1999; accepted March 13, 2000

Measurements have been made of the rate of removal of a solid organic film (phenanthrene) from the surface of a rotating disk using emulsions containing water, the nonionic surfactant Tween 20, and *d*-limonene as the organic phase. The results show that phenanthrene removal initially occurs by the uptake of phenanthrene into the emulsion drops as small aggregates. Simultaneously, the organic phase penetrates into the phenanthrene film, diminishing the adhesive force between the film and the substrate. After sufficient time, the phenanthrene film detaches from the rotating disk surface as a solid. This detachment mechanism accounts for the vast majority of the phenanthrene removal (∼90%). Initial solubilization rates were analyzed using two solubilization models. Both models assume that phenanthrene removal occurs via a mass transfer limited removal of phenanthrene-laden emulsion drops from the phenanthrene film surface into the bulk solution. One model treats the emulsion as homogeneous while the other accounts for the finite size of the emulsion droplets. The latter model was also used to relate the flux of organic phase impacting the phenanthrene film to the detachment times. © 2000 Academic Press

Key Words: **emulsion; cleaning; phenanthrene; solubilization; rotating disk.**

INTRODUCTION

In recent years emulsion cleaners have become more prevalent for removing both solid and liquid organic films from solid substrates. Emulsion cleaners consist of an organic phase dispersed in an aqueous phase; the emulsion is stabilized by surfactants. Emulsion cleaners are less flammable and hazardous than pure organic solvents and give better cleaning performance than aqueous solvents. An additional benefit of emulsion cleaners is their ability to partition into two phases. This often enables the contaminant to be concentrated in one of the phases for disposal, reducing the amount of waste generated (1).

Despite the fact that emulsion cleaners are widely used in practice, there is little understanding of the mechanism for their performance. Klier *et al*. (2) characterized single-phase hydrocarbon-based microemulsions used to remove petroleum jelly from aluminum coupons. They found that both the structure of the microemulsion and its viscosity have a significant effect on cleaning rates.

A number of patents involving emulsion-based cleaners have been assigned (3–9). Many of these emulsion cleaners were developed for cleaning organic residues from metal surfaces. One particular application of interest is the removal of solid tar and oil residues, including asphaltenes, from stainless steel train or tractor trailer tanks used for transporting such materials.

Permsukarome *et al*. (10) measured the kinetics of dissolution of solid asphaltenes in organic solutions of surfactants. They used a differential reactor flow system in which the cleaning solution flowed through a packed bed of asphaltene particles. Asphaltene dissolution behavior was approximated with a first-order rate law. The dissolution kinetics displayed Langmuir–Hinshelwood behavior with respect to the concentration of surfactant. Trends observed suggest that surface desorption rates and mass transfer processes were important factors in the overall rate of asphaltene dissolution.

Prior work by our group has examined the removal of viscous liquid organic films from solid surfaces using aqueous nonionic surfactant solutions (11–16). Related studies have also focused on interfacial and transport phenomena during cleaning in controlled flow systems (17–19). Cleaning studies examined the rate at which the liquid film is removed from the substrate. Because a state of thermodynamic equilibrium does not exist during cleaning processes, our focus was on the cleaning rates as opposed to the amount of contaminant removed at equilibrium. These cleaning rate studies found that as many as three different mechanisms can be responsible for the rate of liquid organic film removal: solubilization, shear removal, and roll up. This work examines removal rates of a solid film of phenanthrene from a solid substrate in order to better understand the mechanisms and key parameters which influence cleaning in emulsion systems. Understanding how these cleaners work might enable more efficient development of effective formulations.

This paper examines the removal rates of a phenanthrene film from a solid surface using emulsion cleaners based on water, Tween 20, and *d*-limonene. The organic film was removed from

[1] To whom correspondence should be addressed. E-mail: ruben@ncsu.edu. Fax: (919) 515-3465.

0021-9797/00 $35.00
Copyright © 2000 by Academic Press
All rights of reproduction in any form reserved.

the surface of a rotating disk in a container of cleaning solution. These experiments enabled the study of organic film removal rates in a controlled hydrodynamic environment where shear rates and mass transfer rates could be estimated. The concentration of the contaminant in the cleaning solution was measured continuously as it was removed from the disk. By measuring the amount of contaminant accumulated in the cleaning solution as a function of time, the rate of cleaning could be determined. Information about the cleaning mechanism was obtained by observing how the cleaning rates changed with disk rotational speed and emulsion composition. Rates of removal were compared with models for the rate of transfer of emulsion drops to the surface. One model treated the emulsion droplets as Brownian particles while the other model accounted for the finite size of the droplets and the interactions between droplets and the surface.

EXPERIMENTAL

Equipment and Protocol

Phenanthrene was chosen as the contaminant because it is a common representative of asphaltene, it is readily obtainable in radioactive form (for detection), and it could be cast into films on solid surfaces. Only one component was used in the contaminant film because different asphaltenes can exhibit different removal rates (14). The solid substrate was chosen to be stainless steel because it is a common surface requiring cleaning in industrial applications.

The phenanthrene was applied to the stainless steel disk from a saturated acetone solution. This solution was prepared by dissolving nonradiolabeled phenanthrene and 100 μCi of ^{14}C-radiolabeled phenanthrene (a total phenanthrene mass of 6.5 g) in excess acetone at 24°C. Once the solution was homogeneous, it was allowed to sit in an open container to allow the acetone to evaporate until the phenanthrene started to precipitate. At this point, the container was sealed. This ensured that the supernatant in the container was a saturated solution of phenanthrene in acetone.

The disks used in the experiments were either 2.20 or 1.25 cm in diameter. Prior to being coated with phenanthrene, the disks were wet sanded by hand with 600-grit sandpaper for approximately 1 min to ensure a reproducible surface. Coating of the disks was performed by heating the disks on an aluminum tray in an oven at 120°C. The disks were then pulled from the oven to a level counter where the acetone/phenanthrene solution, at room temperature, was pipetted onto the hot disks. Volumes of 95 and 250 μL were used to coat the small and large disks, respectively. A larger contaminant solution volume relative to the area of the disk was used for the smaller disks because of increased losses at the disk edge. To obtain an approximately uniform film thickness, once the acetone had evaporated from the films the disks were reheated on the aluminum tray in the 120°C oven to melt the phenanthrene. Disks were then transferred to a 120°C glass tray and removed from the oven. The glass tray was placed on a level counter and the disks were allowed to cool. The resulting films were 116 μm thick (film thickness standard deviation: large disk, 3%, based on 6 different disks; small disk, 22%, based on 13 different disks). The film thickness was estimated by measuring the mass of the phenanthrene film by weighing the disks before and after coating. The density of solid phenanthrene is 1.179 g/cm^3 at 25°C (20). The thickness of the phenanthrene film was calculated assuming the film was a cylinder of uniform thickness with a radius equal to the disk radius.

The emulsion cleaners that are mentioned in the patent literature are a mixture of water with multiple types of surfactants and organic constituents. In order to work with a more simplified model system, only one type of surfactant and organic constituent were used in each emulsion tested. A common organic constituent in emulsion cleaners is *d*-limonene, which is examined in this work. While a variety of surfactants are used in emulsion cleaners, nonionics are prevalent. Tween 20 was used in this work because it is nonionic, a good emulsifier whose properties are known, and readily obtainable.

Cleaning solutions used in these experiments were prepared by first dissolving Tween 20 in deionized water. The *d*-limonene was then stirred into the solution using a magnetic stir plate at high speed, resulting in the formation of a macroemulsion. Final cleaning solutions contained the following mass ratios of water, Tween 20, and *d*-limonene, respectively: 50 : 25 : 25, 50 : 30 : 20, 50 : 20 : 30, 60 : 20 : 20, 70 : 15 : 15, and 64 : 32 : 4. A cleaning solution of only water and Tween 20 in the ratio 67 : 33 was also studied as a base case. This set of emulsion compositions allows the influence of each component to be examined. Solutions with less than 50% water could not be studied because they became too viscous to remain well mixed during the cleaning experiment. Solutions with more than 70% water did not have enough surfactant to stabilize the emulsion during the experiments. If more than approximately 30% surfactant was added to the system, it became too viscous to remain well mixed. Similarly, if more than approximately 30% organic solvent was used, the emulsion was not stable enough and it separated during the experiment.

For some experiments the emulsions were homogenized using a Cyclone Virtishear I.Q. Homogenizer (Virtis) so that the effect of emulsion drop size on cleaning could be determined. As will be shown later, the results obtained in these cleaning experiments are essentially insensitive to the degree of mixing used to prepare the emulsions.

The coated disks were press fit into a Teflon holder with an outer diameter of 4 cm. The holder was submerged into a beaker of cleaning solution. The disks were spun in 500 g of cleaning solution at rotational speeds ranging from 50 to 1750 rpm at 24°C. All rotational speeds used in these experiments were in the laminar flow regime. Additional details on the rotating disk apparatus and its application to cleaning studies are available in previous works (11–15).

For experiments at disk rotational speeds above 250 rpm, contaminant removal detection was performed by hand pipetting

1-cm^3 samples of the cleaning solution at known times during the experiment. Between 15 and 50 of these samples were acquired for each run. These samples were dissolved in 10 cm^3 of UniverSol ES scintillation fluid and analyzed in a Packard 1500 Tri-Carb liquid scintillation analyzer. The 50- and 100-rpm experiments were at such low rotational speeds that the cleaning solution was not well mixed during the experiments. For these low rotational speeds the disks were cleaned for a short period of time (approximately 30 min) and then were removed from the solution. The solution was then mixed thoroughly and sampled for radioactivity. Because the amount of phenanthrene solubilized in the cleaning solution could only be obtained at one point in time, only initial solubilization rates could be obtained at these low rotational speeds.

Solubilities of phenanthrene in limonene and a 67 : 33 mixture of Tween 20 and water were measured. An aliquot of 500 μL of the saturated [^{14}C]phenanthrene acetone solution was pipetted into three separate vials. The vials were allowed to sit open overnight to evaporate the acetone. Once the acetone was evaporated, 500 μL of either limonene or the 67 : 33 Tween 20/water mixture was added to each vial. The vials were sealed and allowed to sit overnight. Samples of 50 μL of the liquid phase in each vial were taken and the amount of phenanthrene present was determined by liquid scintillation analysis. Equilibrium was reached when the concentration of phenanthrene in the liquid phase in the vial did not change for 3 consecutive days. There was always an excess of solid in the vials.

Emulsion Characterization

The emulsions used in the experiments were characterized in terms of the following parameters: viscosity, density, and drop size. The methods used to obtain each of these parameters and the subsequent results follow.

Viscosity. The viscosities for all the cleaning solutions were measured at 24°C using a Rheometrics Dynamic Stress Rheometer (Model SR-200) with a Couette geometry. The Couette flow insert had the following parameters: cup diameter, 31.9 mm; bob diameter, 29.5 mm; bob length, 44.25 mm; and tool inertia, 398.2 g-cm^2. Shear stresses applied ranged from 0.01 to 300 Pa.

All of the emulsions exhibited shear thinning behavior (see Fig. 1). The shaded area corresponds to the range of shear rates used in the rotating disk experiments considering 99% of the disk surface area. The shear rate at the center of the disk is zero and it increases with radial position. Figure 1 shows that over the range of shear conditions used in these experiments, the viscosity remained approximately constant. Viscosity measurements could not be obtained at the higher shear rates due to equipment limitations (exceeding maximum torque of the rheometer). Table 1 lists the average viscosities for the limonene emulsions over the shear rates examined in this work. The viscosities vary significantly with emulsion composition. For the 50% water emulsions (at 24°C), the viscosity nearly doubles as the Tween 20 weight percentage is increased from 20 to 25% and from 25 to 30%. For the emulsions with equal amounts of Tween 20 and limonene, the viscosities decrease with increasing amounts of water. The viscosities of the 60 and 70% water emulsions are very similar, but lower than the viscosities of the 50% water emulsions. The 64 : 32 : 4 emulsion is almost as viscous as the 50 : 20 : 30 emulsion due to its large mass fraction of surfactant.

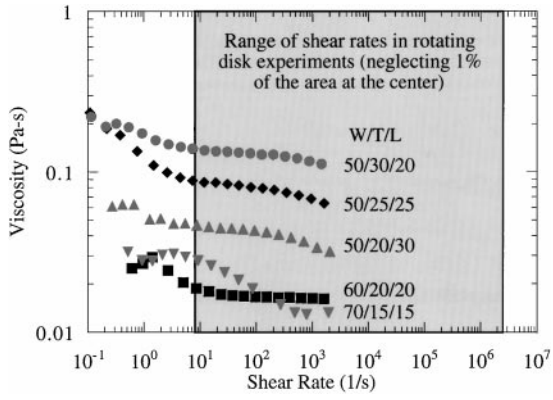

FIG. 1. Shear dependence of viscosity for the limonene emulsions examined in this work.

Density. Emulsion density was determined by weighing 1-cm^3 emulsion samples. A pipette tip was placed in an empty vial and weighed. The pipette tip was used to remove 1 cm^3 of emulsion. The full pipette tip was ejected into the vial and both were weighed. The change in weight corresponds to the mass of emulsion in 1 cm^3 of solution. Five trials were performed for each emulsion composition. There are no significant trends between emulsion density and emulsion composition. All emulsion densities were 1.00 g/cm^3 ±3%.

Drop size. Emulsion drop sizes were determined by viewing 8-μL samples of emulsions on standard glass slides and coverslips under an Olympus BH-2 clinical laboratory microscope. Emulsions were viewed at 400× magnification with the exception of the 70 : 15 : 15 emulsion, which was viewed at both 400× and 100× magnification. All of the emulsion drop sizes were measured after insertion in the rotating disk apparatus for 1 h at 1500 rpm. The measured drop sizes were the same whether the stainless steel disk was initially coated with phenanthrene or used uncoated. This is probably because very small concentrations of phenanthrene are present in the cleaning solution, even

TABLE 1
Viscosity and Average Drop Diameter as a Function of Emulsion Composition

Emulsion composition (wt%) water : Tween 20 : *d*-limonene	Viscosity (Pa-s)	Average drop diam/ standard deviation (μm)
50 : 30 : 20	0.12	2.8/0.9
50 : 25 : 25	0.07	4.0/1.6
50 : 20 : 30	0.035	6.3/2.4
60 : 20 : 20	0.016	9.6/3.5
70 : 15 : 15	0.013	17.9/7.6
64 : 32 : 4	0.033	—

after an entire phenanthrene film is dissolved (approximately 0.05 g phenanthrene/500 g emulsion). Drop size measurements were done for all of the emulsions at 24°C. Drops were too small to view in the 64 : 32 : 4 emulsion. The standard deviations in the drop size measurements are shown in Table 1. The average drop diameters shown in Table 1 are the Sauter-mean diameters.

For the emulsions containing 50% water, the average drop diameters were within an order of magnitude of each other (Table 1). The average drop sizes were larger in emulsions with less surfactant. As the weight percentage of Tween 20 decreased from 30 to 25% and from 25 to 20%, the average drop diameters increased from 2.8 to 4.0 to 6.3 μm. As expected, emulsions with larger drop sizes tended to be less stable.

For emulsions with equal mass fractions of *d*-limonene and Tween 20, each 10% increase in water mass fraction resulted in roughly a doubling of the average drop size. In emulsions with larger amounts of water, more Tween 20 partitioned into the aqueous phase. The concentration of surfactant in the aqueous phase also decreased with increasing water mass fraction. Less Tween 20 was then available to stabilize the *d*-limonene/water interface, resulting in increased interfacial tensions and larger emulsion drops.

In practice, it is difficult to assess the drop sizes that are primarily responsible for cleaning. It is not possible to measure the size of the drops near the surface of the disk before impact nor the size of the drops leaving the disk surface. In order to see how much smaller the emulsion drops could become, the emulsions were homogenized. After homogenization, all of the limonene emulsions had average drop sizes of 1.7 μm. It may be assumed that the emulsion drop sizes in the cleaning solutions were larger than those produced by homogenization because of the much lower shear rates attained in the cleaning experiments. The influence of emulsion drop size on cleaning performance will be discussed later.

While subject to rotational speeds of 250 rpm and higher, the emulsions did not phase separate, even during long periods of shearing (overnight). The duration of lower rotational speed experiments (50 and 100 rpm) was limited due to the stability of the emulsions.

RESULTS AND DISCUSSION

The first two parts of this section present results of cleaning phenanthrene films by pure water and aqueous solutions of Tween 20 (without *d*-limonene). Phenanthrene solubilization into these homogeneous liquids is analyzed by a model that considers the limiting step to be the mass transfer of solubilized phenanthrene from the film surface to the bulk solution. Mass transfer of phenanthrene occurs in molecularly dissolved form in pure water and in the form of micellar aggregates in Tween 20 solutions. The third part presents the cleaning results for the limonene emulsions. The initial cleaning rates in emulsions, which are governed by phenanthrene removal into limonene drops, are analyzed using two solubilization models.

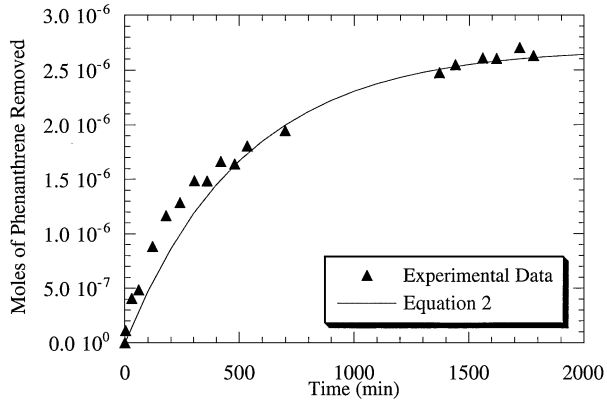

FIG. 2. A cleaning curve using pure water as the solvent at 1000 rpm. Triangles correspond to experimental data points and the curve corresponds to Eq. [2] using a diffusivity from the Wilke–Chang correlation.

The first model treats the emulsions as a homogeneous solution with average fluid properties while the second model accounts for the finite drop sizes in the emulsions.

Pure Water

Figure 2 shows typical experimental data for the removal of a phenanthrene film from the surface of a rotating disk using pure water as the solvent at 1000 rpm. The amount of phenanthrene dissolved as a function of time follows the expected trend of an initially fast rate of removal followed by a decreasing rate until the solution becomes saturated. In this experiment, because of the low solubility of phenanthrene in water, even after the water is saturated with phenanthrene there is still a significant amount of phenanthrene on the disk surface.

The rate at which the phenanthrene dissolves in the water is governed by the mole balance,

$$\frac{dN_p}{dt} = k = \frac{d(C_p V)}{dt} = k_m(C_p^* - C_p)A, \qquad [1]$$

where N_p is the moles of phenanthrene in solution, t is time, k is the initial rate of phenanthrene removal, C_p is the bulk concentration of phenanthrene, V is the volume of the solution, k_m is the mass transfer coefficient of phenanthrene, C_p^* is the solubility of phenanthrene in water, and A is the surface area of the phenanthrene film. Equation [1] assumes that phenanthrene removal is mass transfer limited so that equilibrium is achieved at the interface. Integrating [1] results in an expression for the phenanthrene concentration as a function of time,

$$C_p = C_p^*\left(1 - \exp\left(\frac{-k_m A t}{V}\right)\right). \qquad [2]$$

A relationship for the mass transfer coefficient of single molecules or dilute solutions of Brownian particles (less than 0.1 μm in size) (21) in a Newtonian fluid on a rotating disk flow

geometry was derived by Levich (22),

$$k_m = 0.6205 D_\infty^{2/3} \rho^{1/6} \mu^{-1/6} \omega^{1/2}. \quad [3]$$

Here D_∞ is the diffusion coefficient of phenanthrene in water, ρ is the density of the solution, μ is the bulk solution viscosity, and ω is the rotational speed of the disk. Using the Wilke–Chang correlation (23) the diffusivity of phenanthrene in pure water was estimated as 6.2×10^{-10} m^2/s. Using values of $\rho = 1000$ kg/m^3, $\mu = 0.001$ Pa-s (at 20°C), and $\omega = 104.7$ s^{-1}, k_m was determined to be 4.6×10^{-5} m/s. Figure 2 shows a comparison between [2] and experimental data at 1000 rpm. The following values were used in [2]: $A = 3.80 \times 10^{-4}$ m^2, $V = 5 \times 10^{-4}$ m^3, and $C_p^* = 5.4 \times 10^{-3}$ mol/m^3 (experimentally measured). The model matches the experimental data reasonably well. The agreement between theory and experiment confirms that phenanthrene removal in pure water occurs by molecular solubilization and is mass transfer limited. An additional check on these results is that the experimentally measured solubility of phenanthrene in water at 24°C (5.4×10^{-3} mol/m^3 from Fig. 2 at large times) is in the same range as values previously reported in the literature (7.2×10^{-3} mol/m^3 (24), 6.3×10^{-3} mol/m^3 (25), and 5.6×10^{-3} mol/m^3 (26)).

Aqueous Surfactant Solutions

A typical cleaning curve for a 67 : 33 : 0 (67% water, 33% Tween 20) surfactant solution (at 1000 rpm) is shown in Fig. 3. Since the solubility of phenanthrene in the 67 : 33 : 0 solution (experimentally determined to be 1.7 mol/m^3) is much larger than that in pure water (5.4×10^{-3} mol/m^3) these solutions could not be saturated with the phenanthrene initially present on the disk as in the pure water case. It should be noted that the rate of cleaning is essentially constant with time. After long periods of cleaning (several hours), the phenanthrene film eventually detached from the stainless steel substrate in chunks of various sizes.

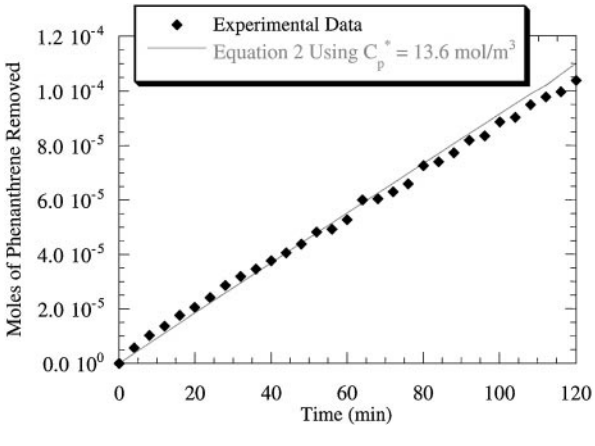

FIG. 3. A typical cleaning curve (67 : 33 : 0 solution at 1000 rpm). The diamonds correspond to experimental data points.

Based on our prior work using aqueous surfactant solutions for removing organic films (11–15), it is likely that the linear phenanthrene removal rate may be controlled by any of the following steps:

(1) transport of surfactant to the interface
(2) adsorption of the surfactant from the solution onto the film
(3) formation of micellar aggregates containing phenanthrene
(4) detachment of the micellar aggregates from the film
(5) transport of the micellar aggregates from the interface to bulk solution

It is not clear a priori which of these steps is controlling, but it will be assumed that either step 1 or 5 is controlling, and the results of this assumption will be compared to experimental data.

Phenanthrene removal rates were examined using Eq. [1]. The diffusion coefficient for the micellar aggregates can be estimated from the Stokes–Einstein relationship (27)

$$D_\infty = \frac{k_B T}{6\pi \mu_W a}, \quad [4]$$

where k_B is Boltzmann's constant, T is temperature, μ_w is the continuous phase viscosity, and a is the particle radius (i.e., the micellar aggregate radius in this case). A value of 2.2×10^{-11} m^2/s was obtained for D_∞ using the following values: $k_B = 1.381 \times 10^{-23}$ J/K, $T = 297$ K, $\mu_w = 0.001$ Pa-s (at 20°C), and $a = 1 \times 10^{-8}$ m. Other known values in Eqs. [2] and [3] are $\rho = 1000$ kg/m^3, $\mu = 0.022$ Pa-s, $A = 3.80 \times 10^{-4}$ m^2, and $C_p \approx 0$. In this case, k_m in Eq. [1] corresponds to the mass transfer coefficient of the micellar aggregates. A plot of Eq. [2] using a C_p^* value fitted to the data of 13.6 mol/m^3 is shown in Fig. 3. Solubility measurements revealed that the solubility of phenanthrene in a 67 : 33 : 0 surfactant solution was 1.7 mol/m^3. The fact that the fitted C_p^* value is significantly greater than the solubilty of phenanthrene in the cleaning solution indicates that phenanthrene is being removed as particulates rather than by micellar solubilization. Calculations based on a C_p^* of 1.7 mol/m^3 would require a diffusivity value of 5.0×10^{-10} m^2/s to fit the data. From the Stokes–Einstein relation (Eq. [4]), this corresponds to a physically unrealistic micellar aggregate radius of 4.4×10^{-10} m.

Small aggregates of the phenanthrene film are likely being removed at the film surface and carried into the bulk solution where they fully dissolve. This is realistic considering that phenanthrene does not form one large uniform crystal upon solidification. Instead, the film contains numerous cracks and voids, consisting of aggregates of small crystals. The surfactant solution can dissolve the crystal boundaries, allowing small aggregates of phenanthrene to be removed.

As will be seen later, experimental k values were found to scale linearly with $\omega^{1/2}$ and have a zero intercept. This behavior is predicted by Eqs. [1] and [3] for $C_p \approx 0$. This linear behavior

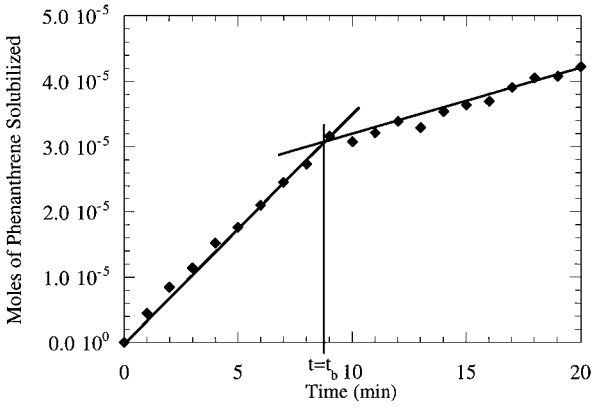

FIG. 4. A typical cleaning curve (50 : 25 : 25 emulsion at 1000 rpm). The diamonds correspond to experimental data points.

means that phenanthrene removal is mass transfer limited in the 67 : 33 : 0 cleaning solution.

Limonene Emulsions

Cleaning behavior. A typical phenanthrene cleaning curve is shown in Fig. 4 for an emulsion containing 50% water, 25% limonene, and 25% Tween 20 at 1000 rpm. The amount of phenanthrene in solution initially increases linearly with time. However, at a given time t_b, the slope of this line decreases abruptly. Analysis of the disks in experiments terminated prior to t_b showed that the phenanthrene film was completely attached to the stainless steel substrate. The disks in experiments stopped after t_b were found to have either the entire phenanthrene film detached from the stainless steel or significant parts of the film missing. In cases where the stainless steel was completely cleaned, it was possible to find the detached film at the bottom of the cleaning solution. It is apparent that the film detaches from the stainless steel substrate at the time corresponding to the change in slope of the cleaning curve. The remaining part of the cleaning curve beyond t_b has no significance, since it is the result of the dissolution of the detached film in the cleaning solution. Since the detached film is either floating in the solution or attached to the side of the beaker, mass transfer rates decrease. The time at which the film detaches from the disk is referred to as the "break-off time," t_b. It is important to note that film detachment was not observed in cleaning experiments with pure water or aqueous solutions of Tween 20.

Figure 5 shows examples of the influence of rotational speed on the cleaning curves for a 50 : 25 : 25 emulsion at 24°C. At higher rotational speeds, the initial slopes of the cleaning curves are larger and the t_b values are smaller. This trend was observed for all of the emulsion compositions examined. The vertical lines indicate the break-off times. The break-off times were shorter for higher rotational speeds, a trend that was also observed for all of the other emulsion compositions examined.

The effect of emulsion drop size on cleaning rates was examined by comparing the initial solubilization rates and break-off times for emulsions with and without homogenization. Recall that all of the emulsions were found to have average emulsion drops sizes of 1.7 μm after homogenization. Results from cleaning experiments at 1000 rpm with the 50 : 25 : 25, 60 : 20 : 20, and 70 : 15 : 15 emulsion compositions were examined. The initial solubilization rates and break-off times did not vary appreciably between the homogenized and nonhomogenized emulsions for the 50 : 25 : 25 and 60 : 20 : 20 emulsion compositions. However, the homogenized 70 : 15 : 15 emulsion exhibited initial solubilization rates that were 50% larger and break-off times that were 50% shorter than those of the nonhomogenized emulsions. With the 50 : 25 : 25 and 60 : 20 : 20 emulsions, the difference in drop size between the homogenized and nonhomogenized emulsions was not significant enough to influence the cleaning results. However, with the 70 : 15 : 15 emulsion, the difference in drop size between the homogenized and nonhomogenized emulsions was significant enough to begin influencing cleaning results. The enhanced cleaning performance of the 70 : 15 : 15 emulsion when subject to homogenization is attributed to the increased contact area between the limonene drops and the phenanthrene film with the smaller droplets. Because the cleaning behavior of the 50 : 25 : 25 and 60 : 20 : 20 emulsions is insensitive to the degree of mixing, homogenization was not used as part of the experimental protocol to prepare the cleaning solutions in this work.

Film characterization. Figure 6 shows photographs of a typical phenanthrene film throughout the cleaning process. Initially, the film has a scaled appearance with cracks or pores on the surface (Fig. 6A). The film is also apparently thinner at the edge of the disk. Small voids and cracks are visible throughout the film. These unavoidable deformities result primarily from the process of solidification of the phenanthrene film as it cools from 120°C to room temperature.

Photographs of the film after brief periods of cleaning (less than 10% of the film has been removed) show that small portions of the film have been removed at the very edge of the disk (Fig. 6B), where small chunks are visible on the surface. This results from solubilization of the film around the film edges which

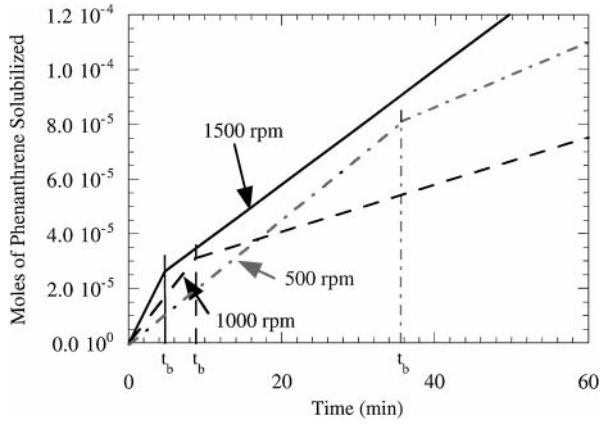

FIG. 5. Cleaning curves for a 50 : 25 : 25 emulsion showing the influence of rotational speed on the initial solubilization rate and break-off times.

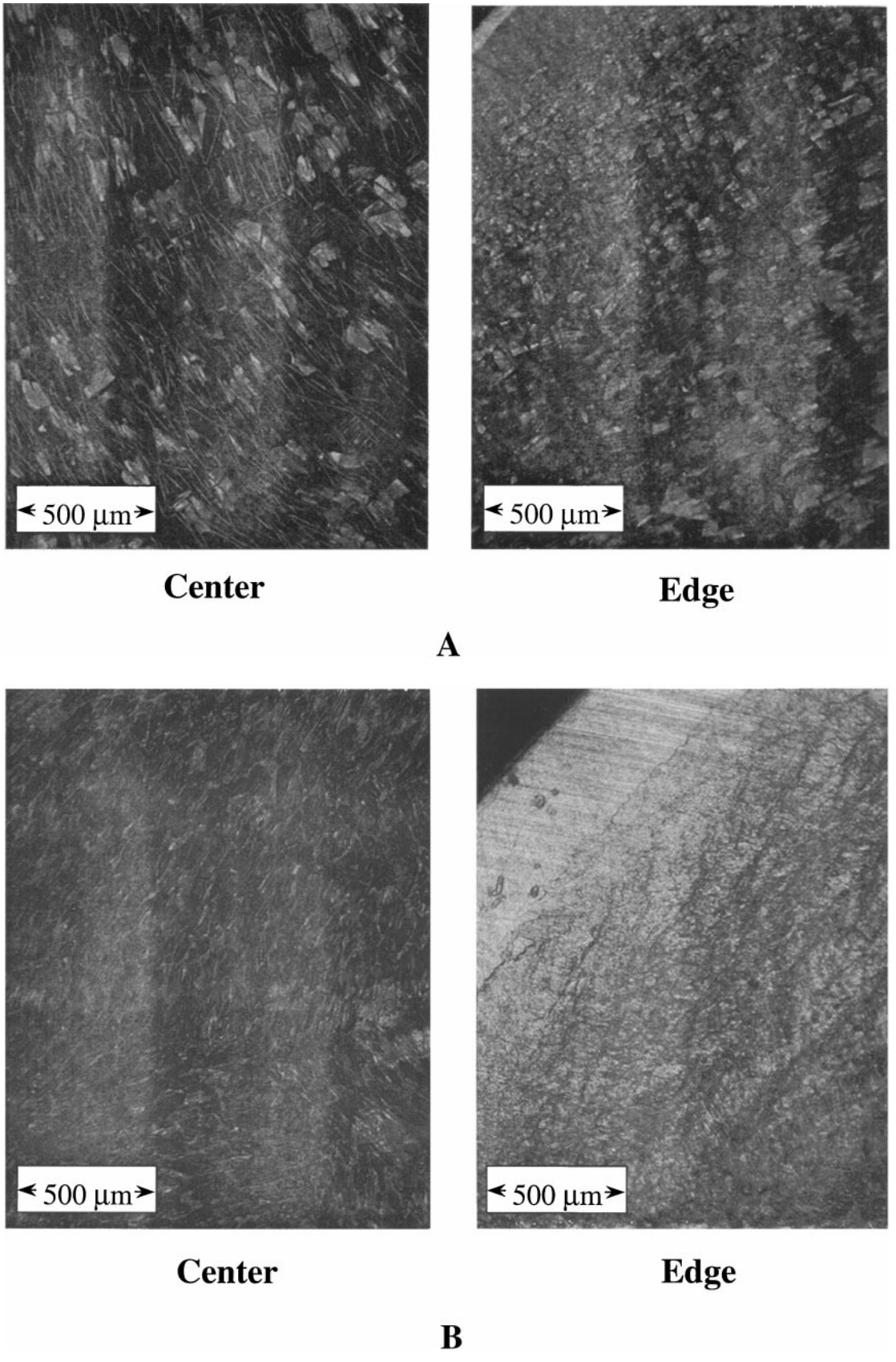

FIG. 6. Photographs of the phenanthrene film: (A) before exposure to the emulsion cleaner and (B) after 6 min of cleaning at 500 rpm with a 50 : 25 : 25 emulsion (large disk).

are initially thin. As the film is solubilized, the thinner parts at the edges can become disengaged from the surface. This effect is not believed to be a significant part of the cleaning mechanism because such a small part of the film is removed in this manner (less than 10%).

In a different series of experiments, 5-μL drops of all of the emulsion compositions were placed on top of phenanthrene coated disks. Upon contact with the cleaning solution, the emulsion drops spread on the upper surface of the film (within the first 15 s) and then penetrated into the phenanthrene film (after approximately 1 min). Upon penetrating, it was possible to see the area where the emulsion drop spread throughout the interior of the film. The presence of *d*-limonene and surfactant facilitated this penetration process since pure water samples were unable to enter the phenanthrene films.

Comparison with solubilization models. The discussion above points to two main phenanthrene removal mechanisms: (i) solubilization and (ii) detachment of the phenanthrene film from the substrate. The substrate is considered clean when the entire phenanthrene film has detached from the substrate. Detachment occurs at $t = t_b$ before the majority of the film has been solubilized. It is important to study both the solubilization and detachment mechanisms since they both play an important role in the removal of phenanthrene from the surface.

In the emulsion, phenanthrene will dissolve primarily inside the limonene drops. The interaction of the limonene drops with the phenanthrene film are postulated to follow the steps shown in Fig. 7:

(1) transport of drops to the interface
(2) contact of the limonene drop with the film
(3) partial penetration of the limonene drop into the phenanthrene film while some of the phenanthrene is taken up into the limonene drop in small aggregates
(4) detachment of the limonene drop from the film
(5) transport of drops from the interface to the bulk solution

It will be assumed that phenanthrene uptake occurs very fast upon contact with the limonene drops. It is not clear a priori which of these steps is controlling, but it will be assumed that steps 2, 3, and 4 are fast, and the results of this assumption will be compared to experimental data. The phenanthrene is believed to be taken up into the limonene drops as small aggregates which eventually dissolve fully in the bulk solution. This is because the phenanthrene film is not a single crystal, but rather many crystals as evidenced by Fig. 6A. The limonene only has to dissolve the edges of a specific crystal in order for it to be removed from the rest of the film.

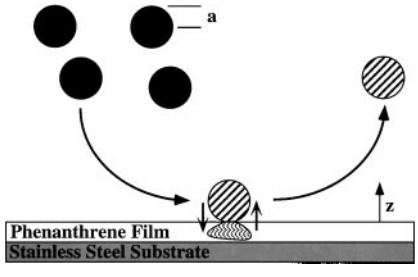

FIG. 7. A schematic of the cleaning mechanism showing the interaction of emulsion drops with the phenanthrene film.

The transport of drops of organic phase to and from the surface is, in general, influenced by buoyancy, hydrodynamic, and surface forces. As a first attempt at modeling this phenomenon, drops are considered Brownian particles, so that their transport is governed by their diffusion and the motion of the fluid in the vicinity of the roatating disk. It will also be assumed that there is no accumulation of limonene drops on the surface of the disk or in the film. This implies that the flux of drops from the bulk solution to the surface of the disk equals the flux of drops away from the disk. This ensures that the number concentration of drops in the emulsion (n_∞) is uniform. After the drops impact the surface of the disk, they become laden with phenanthrene. The flux of phenanthrene-laden drops from the surface of the disk to the bulk solution (where the concentration of phenanthrene-laden drops is negligible) can then be expressed as

$$j = k_{m,l}\, n_\infty, \qquad [5]$$

where $k_{m,l}$ is the mass transfer coefficient for the emulsion drops.

The phenanthrene molar flux j_p is given by

$$j_p = k_{m,l}\, n_\infty V_d C_p^*, \qquad [6]$$

where V_d is the volume of limonene per droplet and C_p^* is the concentration of phenanthrene at the interface. Note that the product $n_\infty V_d$ is equal to ϕ_l, the volume fraction of limonene in the emulsion. Equation [6] assumes that the mass transfer process of phenanthrene removal is due to droplets that carry with them phenanthrene at a concentration C_p^*.

Let the equilibrium concentration of phenanthrene in the bulk emulsion be C_{eq}. If molecular solubilization is responsible for phenanthrene removal, then C_p^* should equal C_{eq}. If the cleaning solution at the interface is indeed homogeneous, then C_p^* cannot exceed C_{eq}. If C_p^* is greater than C_{eq}, it can be inferred that particles of phenanthrene must be present in the cleaning solution as was found in the cleaning of phenanthrene using aqueous surfactant solutions. Values of C_{eq} could not be experimentally determined by equilibrating the emulsions with solid phenanthrene as was done with pure limonene and the 67 : 33 mixture because the emulsions used in this work phase separate prior to equilibration. A value of C_{eq} in the emulsion can be estimated from

$$C_{eq} \cong \phi_l C_l, \qquad [7]$$

where C_l is the solubility of phenanthrene in pure limonene. Tabulated values of C_{eq} for the different emulsions are shown in Table 2.

TABLE 2
Values of C_{eq} and C_p^* Obtained from the Homogeneous Model and Finite Drop Model

Emulsion composition	C_{eq} (mol/m^3)	C_p^* HM (mol/m^3)	C_p^* FDM (mol/m^3)
50 : 30 : 20	7.29	5821	2757
50 : 25 : 25 large disk	8.99	7683	2231
50 : 20 : 30	10.63	10888	1207
60 : 20 : 20	7.22	16358	466
50 : 25 : 25 small disk	8.99	6454	1561

The initial rate of accumulation of phenanthrene in the emulsion (removal rate) is given by

$$\frac{dN_p}{dt} = k = Ak_{m,l}\, n_\infty V_d C_p^*. \quad [8]$$

The flux of limonene droplets to and from the disk surface can be expressed in terms of k by combining Eqs. [5] and [8] to get

$$j = \frac{k}{AV_d C_p^*}. \quad [9]$$

Two models have been used to estimate the mass transfer coefficient $k_{m,l}$ for limonene droplets. The first is a homogeneous model (HM), which treats the emulsion as a homogeneous solution with an effective density and viscosity but with droplets that are not subject to inertial, gravitational, or interfacial forces. The second is a finite drop model (FDM), which accounts for the buoyancy, surface, and body forces acting on the limonene drops as a result of their finite size.

The mass transfer coefficient expression for the HM was presented in Eq. [3] and the corresponding expression for D_∞ is given by Eq. [4]. The only difference in applying these equations for the emulsion case is that D_∞ is the diffusivity of the limonene drops in the emulsion and a is the radius of the limonene drops. The values of viscosities and average drop sizes of the emulsions studied in this work are summarized in Table 1.

Combining Eqs. [3] and [8], the following expression is obtained for the initial rate of phenanthrene solubilization using the HM:

$$k = 0.6205AD_\infty^{2/3}\rho^{1/6}C_p^* n_\infty V_d \mu^{-1/6}\omega^{1/2}. \quad [10]$$

Since the emulsion drops are larger than what are normally considered to be Brownian particles and may be influenced by body and surface forces, the FDM approach will also be used to estimate the value of $k_{m,l}$ to take these effects into account. The FDM estimates the $k_{m,l}$ values using the theory developed by Dabros *et al*. (28) for the deposition of non-Brownian spheres onto rotating disk surfaces taking gravity, London–van der Waals, and hydrodynamic forces into account (21, 28, 29). These calculations consider a dilute solution of spherical particles in which there are no particle–particle interactions.

The original paper of Dabros *et al*. (28) and two accompanying papers by Adamczyk and co-workers (21, 29) contain several typographical errors in the equations. Specifically, the definition of the Grashof number, Gr, is incorrect in (21, 28, 29). The corrected equations are presented in the Appendix, using the same nomenclature as in these earlier works. From these works, the flux of particles to the disk surface can be calculated from the expression (29)

$$j = \frac{D_\infty n_\infty}{a} F_1(\bar{\delta})\left(\frac{d\bar{n}}{dH}\right)_{\bar{\delta}}, \quad [11]$$

where n_∞ is the particle number concentration far from the disk (i.e., in bulk solution as with the HM), a is the particle radius, $\bar{\delta}$ is the dimensionless closest distance possible between a droplet and the disk surface, F_1 is a function of vertical distance from the disk surface (see Appendix), $\bar{n}$ is the dimensionless particle concentration, and H is the dimensionless vertical distance from the disk surface. The mass transfer coefficient for the limonene drops predicted by the FDM can be calculated from Eqs. [5] and [11],

$$k_{m,l} = \frac{D_\infty}{a} F_1(\bar{\delta})\left(\frac{d\bar{n}}{dH}\right)_{\bar{\delta}}. \quad [12]$$

In comparing the mass transfer coefficient expressions from the HM (Eq. [3]) and the FDM (Eq. [12]) one can see that the HM contains an explicit dependence on density, viscosity, and rotational speed. The FDM depends on these parameters implicitly and the particle radius explicitly.

Initial rates of phenanthrene solubilization, k, were calculated with the FDM by combining Eqs. [8] and [12] to obtain

$$k = A\frac{D_\infty}{a} F_1(\bar{\delta})\left(\frac{d\bar{n}}{dt}\right)_{\bar{\delta}} n_\infty V_d C_p^*. \quad [13]$$

As with the HM, here it is assumed that phenanthrene uptake by the limonene drops occurs instantaneously upon contact.

Having presented the HM and FDM, we now compare these models with experimental solubilization data. Equation [10] predicts that k depends linearly on $n_\infty V_d/\mu^{1/6}$ for a given ω. The experimental trends are shown in Fig. 8A for all of the limonene emulsions tested. The lines correspond to linear curve fits passing through the experimental data for each of the three rotational speeds shown. However, the data do not exhibit a zero intercept as predicted by Eq. [10] because this equation assumes that phenanthrene removal occurs only by the limonene drops. In reality, phenanthrene is also removed by surfactant in the aqueous phase. At higher values of $n_\infty V_d/\mu^{1/6}$, there is less surfactant present in the aqueous phase because it is present at the aqueous/organic phase interface, stabilizing the emulsion. Under these conditions removal by the aqueous phase is not

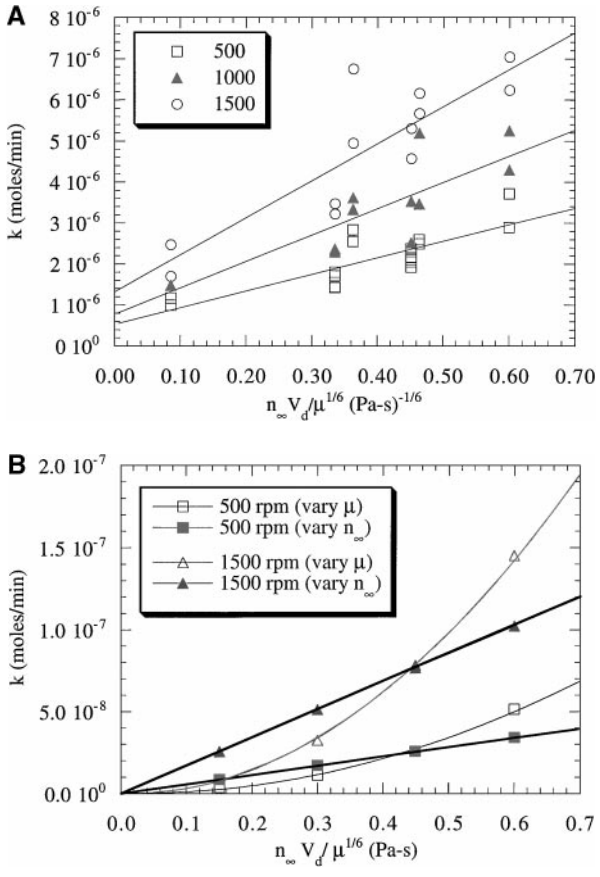

FIG. 8. The dependence of initial solubilization rate on $n_\infty V_d/\mu^{1/6}$ for (A) the six limonene-based emulsions at 24°C (experimental data shown) and (B) the FDM for theoretical emulsions with $a = 2\,\mu$m. Solid data points correspond to theoretical emulsions with $\mu = 0.07$ Pa-s and variable n_∞. Hollow data points correspond to theoretical emulsions with fixed $n_\infty V_d = 0.29$ and variable viscosity. Curves corresponding to 500 and 1500 rpm are shown.

significant. At lower values of $n_\infty V_d/\mu^{1/6}$, the surfactant concentration is higher in the aqueous phase and little limonene is present to remove phenanthrene. Here removal by micellar aggregates is more significant. Because most of the experiments in this work are done at larger values of $n_\infty V_d/\mu^{1/6}$, the rate of removal in the emulsions by micellar aggregates is neglected.

The dependence of the FDM on the parameter $n_\infty V_d/\mu^{1/6}$ (Eq. [13]) is not as obvious as in the HM. Figure 8B shows calculated k values for a series of theoretical emulsions with $V_d = 3.35 \times 10^{-17}$ m^3. The straight lines with the solid symbols correspond to k values obtained for theoretical emulsions with a viscosity of 0.07 Pa s as the parameter n_∞ was varied. The curves with the hollow symbols correspond to k values obtained for theoretical emulsions with a fixed value of n_∞ of 8.65×10^{15} drops/m^3 while the viscosity was varied. With both approaches the FDM exhibits an increase in k with increasing $n_\infty V_d/\mu^{1/6}$. In practice, changes in n_∞ will affect μ and vice versa. While the dependence of n_∞ on μ is not known, the two cases shown here should serve as a guide to how the FDM k values depend on $n_\infty V_d/\mu^{1/6}$.

TABLE 3

Dependence of $n_\infty V_d/\mu^{1/6}$ (from Eq. [10]—Property of Emulsion Composition) and $k\omega^{-1/2}$ (from Eq. [10]–Dependence of Solubilization Rate on Rotational Speed) on Emulsion Properties

Emulsion composition	$n_\infty V_d/\mu^{1/6}$ (Pa-s)$^{-1/6}$	$k\omega^{-1/2}$ (mol-s$^{-1/2}$)
50 : 30 : 20	0.335	4.2×10^{-9}
50 : 25 : 25	0.452	5.9×10^{-9}
50 : 20 : 30	0.600	8.2×10^{-9}
60 : 20 : 20	0.464	7.2×10^{-9}
70 : 15 : 15	0.363	6.4×10^{-9}
64 : 32 : 4	0.086	2.6×10^{-9}
67 : 33 : 0	0	1.5×10^{-9}

The HM predicts an increasing linear dependence of k on $\omega^{1/2}$. Table 3 lists experimental values of $k/\omega^{1/2}$ obtained from linear curve fits passing through the origin of the experimental data. Equation [10] can be solved for C_p^* using the values shown in Tables 1, 3, and 4. Such a calculation gives the C_p^* values shown in Table 2. The problem with the HM is that the molar density of solid phenanthrene is 6615 mol/m^3, which is smaller than most of the values obtained for C_p^* from the experimental data. The 70 : 15 : 15 emulsion C_p^* value is a factor of 4 larger than the molar density of solid phenanthrene. The HM should not be applied to these emulsions because the emulsion drops are too large to be considered Brownian particles. Despite the shortcomings of the HM, this theory seems to predict proper trends of k with $n_\infty V_d/\mu^{1/6}$ and $\omega^{1/2}$. Because the HM cannot be applied quantitatively to these emulsions, all further discussion will focus on the FDM.

Figure 9 shows how experimental k values compare with the FDM over the range of rotational speeds examined in this work for the 50 : 25 : 25 emulsion. The FDM exhibits the same trend of increasing k with $\omega^{1/2}$. However, k does not increase linearly with $\omega^{1/2}$ as predicted by the HM model. A value of

TABLE 4

Values Used in the FDM in Fig. 8B to Calculate j

Parameter	Value
A	3.80×10^{-4} m^2
ρ_{water}	1000 kg/m^3
μ	0.07 Pa-s
k_B	1.381×10^{-23} J/K
T	297 K
μ_w (to calculate D_∞)	0.001 Pa-s
a	2×10^{-6} m
C_p^*	31 mol/m^3
$\Delta\rho = \rho_{water} - \rho_{limonene}$	159.8 kg/m^3
g	9.8 m/s^2
δ (dimensionless)	0.01
V_d (based on $a = 2 \times 10^{-6}$ m)	3.35×10^{-17} m^3
Ad (between emulsion drops)	0.4 (28)
A_H (calculated from Ad using k_B and T above)	1.64×10^{-21} J
λ/a	0.28 (28)

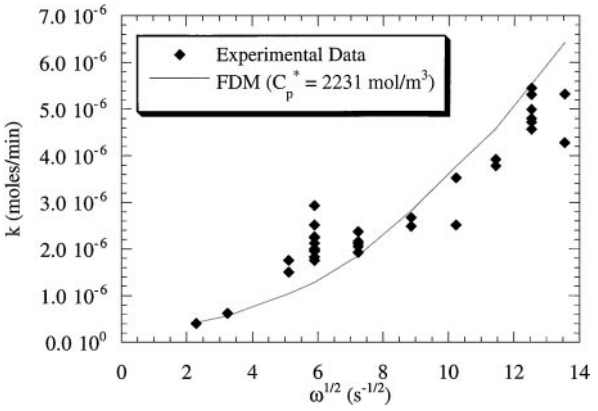

FIG. 9. A comparison of initial solubilization rate on rotational speed between experimental data with the FDM predictions (50 : 25 : 25 emulsion at 24°C, $C_p^* = 2231$ mol/m^3).

$C_p^* = 2231$ mol/m^3 was obtained by minimizing the error between the experimental and FDM k values. Table 2 lists values of C_{eq} and C_p^* obtained from the other emulsions. While there does not appear to be a strong trend in C_p^* with emulsions composition, it appears that in general larger surfactant concentrations and larger mass fractions of water tend to increase C_p^*. The scatter associated with these C_p^* values can be seen by comparing the 50 : 25 : 25 emulsion results for the large and small disks. The small disk C_p^* is 30% smaller than that for the large disk. Values of C_p^* for all of the emulsions are below the molar density of solid phenanthrene.

Figure 10A compares best fit lines through experimental k vs $\omega^{1/2}$ data for the cleaning solutions at 24°C. The error bars correspond to a standard deviation of the slope of the curve fit to the experimental data. These slopes are summarized in Table 3. The larger slope corresponds to faster initial solubilization rates. Among the 50% water emulsions, those with more limonene clean faster. This trend in cleaning rates obeyed the same dependence with $n_\infty V_d/\mu^{1/6}$, reaching a maximum at the 50 : 20 : 30 emulsion composition. By comparing the 67 : 33 : 0 curve with the five emulsions studied, it is apparent that the limonene significantly enhanced initial removal rates compared to water/Tween 20. It is believed that solubilization into the aqueous phase is less significant in the presence of the limonene because more of the surfactant is at the water/limonene interface rather than in micellar aggregates where it can solubilize phenanthrene.

By comparing the emulsions with equal mass fractions of Tween 20 and limonene in Fig. 10B, we can see that more concentrated Tween 20/limonene solutions do not necessarily give faster solubilization rates. The 60% water emulsion exhibited faster solubilization rates than the 50% water emulsion. This is likely due to the higher viscosity of the 50% water emulsion. The 70% water emulsion did not clean as well as the 60% water emulsion because there was less limonene present in the system. The 70% water emulsion performed better than the 50% water emulsion.

As previously stated, the initial solubilization of the phenanthrene film typically only accounts for about 10% of the phenanthrene removal in this system under the range of conditions examined. The majority of the phenanthrene is removed when the film detaches from the substrate. By using Eq. [9] with the best fit values of C_p^* to represent experimental k values, we estimated the flux of emulsion droplets at the disk surface. We now examine the detachment mechanism by relating the amount of time

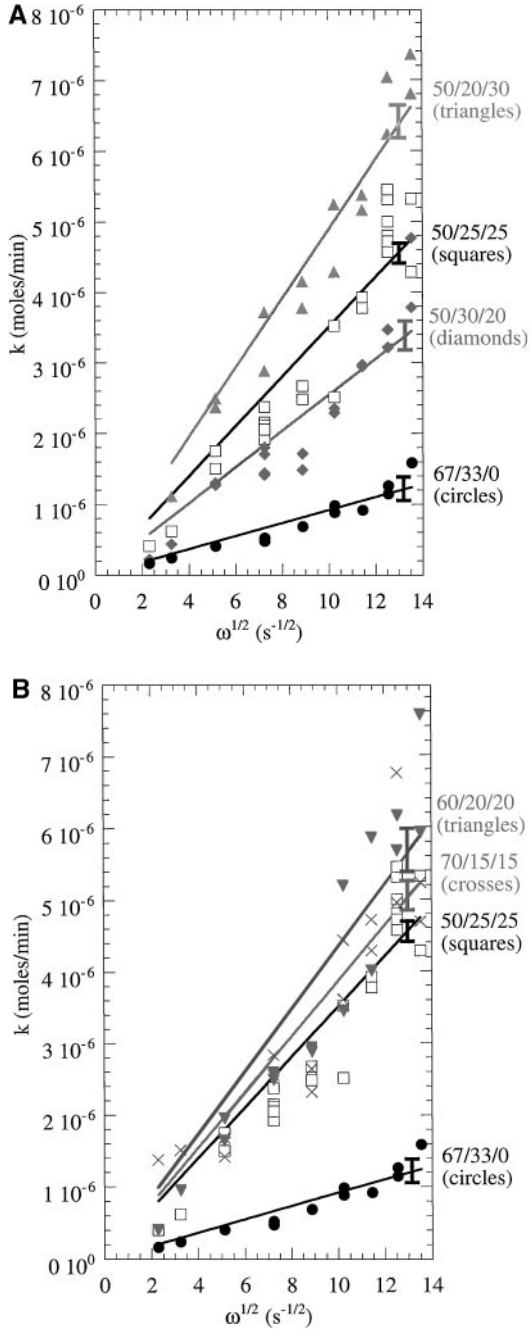

FIG. 10. The dependence of initial solubilization rate on rotational speed for (A) 50% water emulsions and (B) emulsions with equal mass fractions of Tween 20 and limonene.

needed for the phenanthrene film to detach to the number of emulsion droplets that have impacted the film.

Break-off times. Due to the rotational motion of the disk, the fluid exerts a net torque on the phenanthrene film. Note that the net force that the fluid exerts on the disk is zero due to the symmetry in the flow field. However, the net torque is nonzero and it opposed the rotating motion. Since the angular momentum of the film is constant, this torque is compensated at the surface by the total torque needed to overcome adhesion forces. The torque that this surface can withstand will decrease uniformly during the solubilization stage due to a reduction in the adhesion of the phenanthrene to the stainless steel interface resulting from the presence of limonene that penetrates the film. At the break-off point, one can postulate that the applied torque will equal the torque needed to overcome adhesion forces,

$$|\boldsymbol{\tau}_{\text{shear}}| = |\boldsymbol{\tau}_{\text{adhesion}}|. \quad [14]$$

In earlier work (13), the shear stress vector along the surface of a rotating disk, $\mathbf{t}_s$, was shown to be

$$\mathbf{t}_s = [0.510\mathbf{e}_r - 0.616\mathbf{e}_\theta](\mu\rho)^{1/2} r\omega^{3/2}, \quad [15]$$

where $\mathbf{e}_r$ and $\mathbf{e}_\theta$ are unit vectors in radial and angular directions, respectively. The torque exerted by this shear stress is given by

$$\boldsymbol{\tau}_{\text{shear}} = \int \mathbf{r} \times \mathbf{t}_s \, dA, \quad [16]$$

where $\mathbf{r}$ is radial position along the disk and A is the disk area. Combining Eqs. [15] and [16] and integrating over the disk surface result in an expression for the magnitude of the shear torque,

$$|\boldsymbol{\tau}_{\text{shear}}| = 0.308\pi(\mu\rho)^{1/2} R^4 \omega^{3/2}, \quad [17]$$

where R is the disk radius.

The torque needed to overcome adhesive forces can be calculated from the stress of adhesion, $\boldsymbol{\sigma}_{\text{adhesion}}$, by the expression

$$\boldsymbol{\tau}_{\text{adhesion}} = \int \mathbf{r} \times \boldsymbol{\sigma}_{\text{adhesion}} \, dA. \quad [18]$$

The stress of adhesion is the force/area that needs to be applied to detach the film at a given point. Since it is in the presence of limonene that film detachment is observed, we postulate that the magnitude of $\boldsymbol{\sigma}_{\text{adhesion}}$ decreases during the experiment because of dissolution of the phenanthrene at the stainless steel interface by the limonene that has penetrated into the film. It will be assumed that the rate at which $\boldsymbol{\sigma}_{\text{adhesion}}$ decreases with time is directly proportional to the amount of limonene that penetrates into the film. This can be expressed by the relation

$$|\boldsymbol{\sigma}_{\text{adhesion}}| = \sigma_o - \beta j A t, \quad [19]$$

where σ_o is the initial stress of adhesion of the phenanthrene film in the emulsion, β is the change in the stress of adhesion per emulsion droplet, and t is time. The product jA gives the total number of droplets hitting the surface per unit time. If it is assumed that $|\boldsymbol{\sigma}_{\text{adhesion}}|$ is uniform across the entire disk, combining Eqs. [18] and [19] and integrating result in a time-dependent torque,

$$|\boldsymbol{\tau}_{\text{adhesion}}| = \frac{2}{3}\pi R^3(\sigma_o - \beta j A t). \quad [20]$$

At the break-off time, $t = t_b$ and Eq. [20] can be combined with Eq. [14] to give

$$j A t_b = \frac{\sigma_o}{\beta} - \frac{1}{\beta}\left(\frac{3}{2\pi R^3}\right)|\boldsymbol{\tau}_{\text{shear}}|. \quad [21]$$

Equation [21] predicts a linear relationship between jAt_b and $|\boldsymbol{\tau}_{\text{shear}}|$. The parameter β can be obtained from the slope and σ_o from the intercept of the best fit line through the experimental data. If true, this relationship should fit data with different disk radii and rotational speeds.

Figure 11 is a graph of jAt_b versus $|\boldsymbol{\tau}_{\text{shear}}|$ for the large-diameter disks (0.022-m diameter). Data points correspond to the average of the experimental data and the errors bars correspond to one standard deviation from the average. The linear curve fits shown for each data set are based on the average data points. In Fig. 11, values of j were obtained from Eq. [9] using experimental k values and C_p^* best fit values from the FDM. Both A and $|\boldsymbol{\tau}_{\text{shear}}|$ were calculated using the parameters $R = 0.011$ m, μ from Table 1, and $\rho = 1000$ kg/m^3, and t_b is the experimental break-off time. The jAt_b results in Fig. 11 show a decreasing trend with increasing $|\boldsymbol{\tau}_{\text{shear}}|$ despite significant scatter.

The β and σ_o values (see Table 5) were obtained from the slope and intercept of the curve fits. From Fig. 11, β values were obtained that range from $O(10^{-7}$ to 10^{-6} N/drop m^2) and σ_o values range from $O(10$ to 100 N/m^2). The σ_o values seem reasonable when one realizes that they are for the films exposed to the emulsions. To put these numbers in perspective, a calculation of the

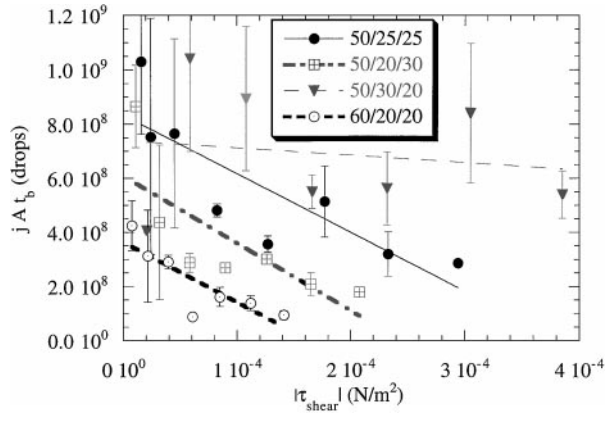

FIG. 11. A comparison of jAt_b for large disks with $|\boldsymbol{\tau}_{\text{shear}}|$ for several of the limonene emulsions at 24°C. The j values were obtained from Eq. [9] with experimental k values.

TABLE 5
Values of β and σ_o Obtained from Eq. [20] Using j Values from Eq. [9] with Experimental k Values

Emulsion composition	β (N/drop-m^2)	σ_o (N/m^2)
50 : 25 : 25 large disk	1.65×10^{-7}	138
50 : 20 : 30	1.44×10^{-7}	88
50 : 30 : 20	1.32×10^{-6}	978
60 : 20 : 20	1.62×10^{-7}	59
50 : 25 : 25 small disk	1.75×10^{-7}	91

stress required to slide a steel disk across a flat steel surface requires a stress on the order of 100 N/m^2. Because of the scatter, it is difficult to determine which emulsion provides better results by this detachment mechanism, but the results shown in Table 5 give an idea of the order of magnitude of β and σ_o. The scatter likely results from the variation from run to run in the way the phenanthrene film crystallizes and adheres to the surface. Experiments with a greater local control of this would be needed to quantitatively validate the model presented here. However, the model proposed explains the trend observed in the experimental data.

In order to see if the theory gives the proper scaling with R, results with disks of a smaller radius ($R = 0.00625$ m) were examined. Holders were fabricated that were identical to those used with larger disks except that the cut out for the disk was smaller. This way the hydrodynamic conditions were kept the same for both the small and large disks. From these experiments, the initial rates of solubilization, when adjusted for the film surface area, were the same for both the large and small disks as expected (see Fig. 12).

Figure 13 compares jAt_b values as a function of $|\tau_{shear}|/R^3$ for the large and small disks cleaned with a 50 : 25 : 25 emulsion. The jAt_b values shown are based on all of the experimental data obtained for both sized disks. The same trend as in Fig. 11 of decreasing jAt_b with increasing $|\tau_{shear}|$ is seen. Table 5 shows β and σ_o values for the small disks. The large and small disk β values differ by only 6% and the σ_o values by 34%. This is

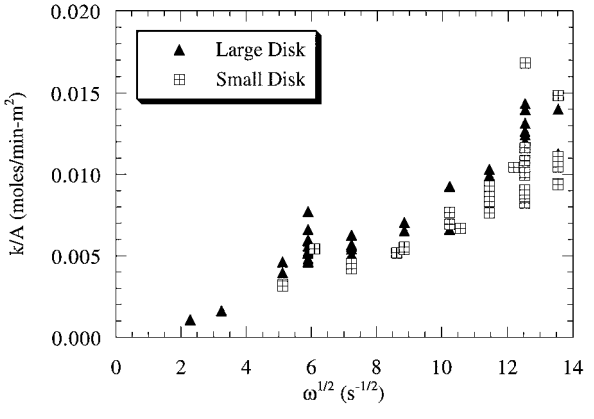

FIG. 12. A comparison between small and large disk initial solubilization rates with rotational speed (50 : 25 : 25 emulsion at 24°C).

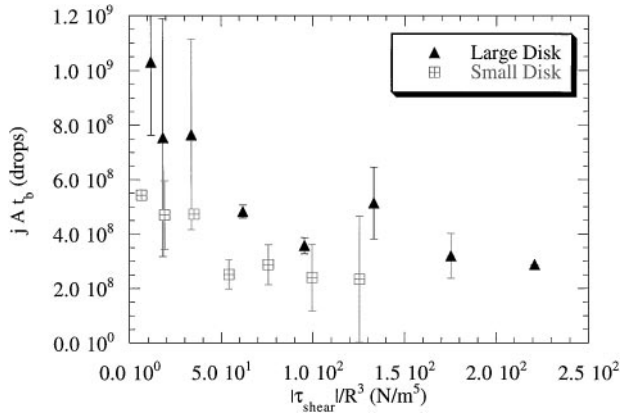

FIG. 13. A comparison of jAt_b for small disks with $|\tau_{shear}|/R^3$ for the 50 : 25 : 25 limonene emulsion at 24°C. The j values were obtained from Eq. [9] with experimental k values.

very good agreement considering the degree of scatter associated with the experiments.

In order to determine the influence of disk radius on the break-off time, experiments were done with both small and large disks subject to the same $|\tau_{shear}|$. Ten duplicate experiments were performed with large disks at 332 rpm and small disks at 1500 rpm (50 : 25 : 25 emulsion, 24°C). From these experiments, it was found that the mean break-off time for the large disks is 26.9 min (standard deviation of 15.3 min) and 11.0 min (standard deviation of 6.7 min) for small disks. The ratio of these average experimental break-off times is $t_{b,l}/t_{b,s} = 2.45$, where the indices indicate l for large disk and s for small disk. Because β, σ_o, and $|\tau_{shear}|$ are the same for both the small and the large disk experiments being compared, Eq. [21] can be used to obtain the following relationship $j_{large}A_{large}t_{b,large} = j_{small}A_{small}t_{b,small}$:

$$j_l A_l t_{b,l} = j_s A_s t_{b,s}. \qquad [22]$$

According to Eq. [22], j values can be used to find the expected ratio of the large to small disk break-off times. Recall that A is known for both size disks and j can be obtained using experimental k values with Eq. 9. This gives a value of $t_{b,l}/t_{b,s} = 1.02$. This differs from the experimentally observed value by roughly a factor of 2, which we attribute to scatter in the data. The model seems to predict the correct trends.

Another useful comparison is to see how the total volume of emulsion drops which have impacted the film prior to break-off (V_{drops}) compares with the volume of the phenanthrene film (V_{film}). Phenanthrene film volumes were 4.4×10^{-8} m^3 for large disks and 1.4×10^{-8} m^3 for small disks. The total drop volume was calculated from the number of drops that have penetrated the film at break off (jAt_b) and the size of the drops measured experimentally (Table 1). The ratio V_{drops}/V_{film} tells how effective the emulsion is at causing the phenanthrene film to detach from the stainless steel. That is, at a given rotational speed, an emulsion with a smaller V_{drops}/V_{film} is more effective than an emulsion with a larger V_{drops}/V_{film} value.

TABLE 6
Ratio of V_{drops} Prior to t_b to V_{film} as a Function of Emulsion Composition and Rotational Speed

ω (rpm)	V_{drops}/V_{film} 50 : 25 : 25 large disk	V_{drops}/V_{film} 50 : 25 : 25 small disk	V_{drops}/V_{film} 50 : 20 : 30	V_{drops}/V_{film} 50 : 30 : 20	V_{drops}/V_{film} 60 : 20 : 20
250	0.25	0.41	0.82	0.03	1.42
332	0.18	—	—	—	—
500	0.19	0.36	0.41	0.09	1.05
750	0.12	0.36	0.27	0.07	0.97
1000	0.09	0.19	0.25	0.05	0.30
1250	0.12	0.23	0.28	0.05	0.54
1500	0.08	0.18	0.20	0.07	0.46
1750	0.07	0.18	0.17	0.04	0.31

The 50 : 25 : 25 limonene emulsion results for the large and small disks both show a decrease in V_{drops}/V_{film} with increasing rotational speed. One would expect this trend because larger rotational speeds produce a larger $|\boldsymbol{\tau}_{shear}|$. Values of V_{drops}/V_{film} for the smaller disk are roughly double those of the larger disk. This suggests that the emulsion is more effective for larger disks at a specific rotational speed. This can be explained because the larger disk is subject to a larger $|\boldsymbol{\tau}_{shear}|$.

Of the limonene emulsions shown in Table 6 for large disks at 24°C, the results suggest that the 50 : 30 : 20 emulsion is most effective. The value of V_{drops}/V_{film} for this emulsion is the smallest at all of the rotational speeds. This is an unexpected result because the 50 : 30 : 20 emulsion has the slowest solubilization rate of all the five emulsions examined. However, the effectiveness is based on the volume of limonene that needs to impact the film to cause break-off. The 50 : 30 : 20 emulsion is the most viscous of all the emulsions examined. At a given rotational speed, this emulsion will exert the largest $|\boldsymbol{\tau}_{shear}|$ on the phenanthrene film, which will result in break-off at larger $|\boldsymbol{\sigma}_{adhesion}|$ values. Break-off is influenced not only by the amount of limonene drops that have impacted the surface, but also by the amount that the initial stress of adhesion needs to be decreased.

CONCLUSIONS

The initial removal rate of phenanthrene from a stainless steel substrate was found to be controlled by the uptake of phenanthrene aggregates into emulsion droplets. While the phenanthrene solubilized, the limonene likely decreases the stress of adhesion between the phenanthrene film and the stainless steel. When enough of the organic phase has been absorbed by the film so that the stress of adhesion has been sufficiently reduced, the phenanthrene film detaches from the substrate. This break-off mechanism accounts for the vast majority of the phenanthrene removal (~90%). It was also found that the initial solubilization rates were related to the emulsion viscosity and organic-phase volume fraction while no clear trend exists between these parameters and the break-off times. Larger concentrations of surfactant and organic component in the emulsion do not necessarily correspond to faster solubilization rates or shorter break-off times. Measured solubilization rates were analyzed using both a homogeneous model and a finite droplet model of mass transfer at the disk surface. The break-off time and flux of emulsion droplets to the disk surface were found to be related to the torque of shear exerted on the phenanthrene film by the bulk cleaning solution. Within the degree of scatter associated with these experiments it was found that all of the emulsions induce break-off equally fast.

APPENDIX

The following is a summary of the key equations used in the FDM developed by Dabros *et al*. (28) and Adamczyk and co-workers (21, 29). In the expressions that follow, n is the local particle number concentration; n_∞, the particle number concentration far from the disk (i.e., in bulk solution as with the HM); z, perpendicular distance of the drop center from the disk surface; δ, the closest distance possible between a droplet and the disk surface; and $f(0)$, the "universal constant" for the rotating disk, 0.510 (28). The following dimensionless variables can be defined:

$$\bar{n} = \frac{n}{n_\infty} \qquad [A.1]$$

$$H = \frac{z}{a} - 1 \qquad [A.2]$$

$$\bar{\delta} = \frac{\delta}{a} \qquad [A.3]$$

$$\mathrm{Pe} = 2f(0)\frac{\omega^{3/2}a^3}{\nu^{1/2}D_\infty} \qquad [A.4]$$

$$\mathrm{Gr} = \frac{2\Delta\rho g}{9f(0)\omega^{3/2}\mu^{1/2}\rho^{1/2}}. \qquad [A.5]$$

A cylindrical coordinate system is used where the origin is the center of the surface of the rotating disk. Because the disk is facing down during the experiments, the direction of increasing z is away from the disk surface in the direction of gravity. The viscosity values in the Pe and Gr expression are those of the bulk solution; in our case these are the viscosities of the emulsions as shown in Fig. 1. As with the HM, the viscous terms arise due to the flow field of the bulk solution around the rotating disk. The particle continuity equation can be used to obtain two equations that relate $\bar{n}$, the dimensionless particle concentration, to the dimensionless vertical distance from the surface of the disk (28):

$$\frac{d\bar{n}}{dH} = -\left\{\frac{1}{2}\mathrm{Pe}[(H+1)^2F_2 + \mathrm{Gr}] + \mathrm{Ad}\frac{(\lambda/a + 22.232H)\lambda/a}{H^2(\lambda/a + 11.116H)}\right\}\bar{n} + \frac{j_H}{F_1} \qquad [A.6]$$

$$\frac{dj_H}{dH} = \mathrm{Pe}(H+1)F_3\bar{n}. \qquad [A.7]$$

Here Ad is the dimensionless adhesion number (A_H/k_BT), where A_H is the Hamaker constant between the droplet and the disk surface through the cleaning solution, j_H can be treated as the H component of the particle flux vector, and λ is a constant that accounts for the reduction in London forces between the particles and the disk surface due to the surrounding medium (about 10^{-5} cm for water) (28, 30). Values for these parameters are given in Table 4. In Eqs. [A.6] and [A.7], the terms with the Pe are hydrodynamic terms, Gr is the buoyancy term, and Ad is the Van der Waals forces term.

The functions F_1, F_2, and F_3 only depend on vertical position,

$$F_1 = \frac{H}{H+1}$$
$$F_2 = \frac{2.23(H+1)-H}{(H+1)^2} + 1 \qquad \text{[A.8]}$$
$$F_3 = 1 - \frac{5}{16(H+1)^3}.$$

Equations [A.6] and [A.7] are subject to the boundary conditions:

$$\bar{n} = 0 \text{ for } H = \bar{\delta}$$
$$\bar{n} = 1 \text{ for } H \to \infty. \qquad \text{[A.9]}$$

The first boundary condition specifies that at a vertical distance from the disk a little large than the particle radius, the particle concentration in solution is zero. In other words, very close to the disk the particles are all attached to the disk. The second boundary condition states that the particle concentration far from the disk is equal to that in the bulk solution.

In order to convert this boundary value problem to an initial value problem, the second boundary condition can be replaced with a prescribed value for j_H at $H = \bar{\delta}$. The solution to these equations is iterative, requiring a guess for an initial value of j_H. The correct value of j_H is the one that will result in $\bar{n} = 1$ for large H. This approach was used to solve Eqs. [A.6] and [A.7] numerically.

ACKNOWLEDGMENTS

This work was funded by National Science Foundation Grants CTS-9216850 and CTS-9616638 and Corpex Technologies in Research Triangle Park, NC. A special thanks to Dr. Peter Kilpatrick and Andy Sullivan for allowing use of the microscope for emulsion drop size measurements and the homogenizer. Thanks also to Dr. Saad Khan, Bor-Sen Chiou, and Jenny Shay for allowing use of the rheometer.

REFERENCES

1. D'Ruiz, C. D., "Aqueous Cleaning as an Alternative to CFC and Chlorinated Solvent-Based Cleaning," Noyes, Park Ridge, 1991.
2. Klier, J., Suarez, R. S., Green, D. P., Kumar, A. M., Hoffman, M., Tucker, C. J., Landes, B., and Redwine, D., *J. Am. Oil Chem. Soc.* **74,** 861 (1997).
3. D'Muhala, T. F., and Zietlow, T. C., "Terpene-Based Cleaning Composition," U.S. Patent 5,663,135, 1997.
4. Farnsworth, A. M., "Cleaning Composition," U.S. Patent 3,933,674, 1976.
5. Hart, P. R., "Refinery Vessel Cleaning Treatment," U.S. Patent 5,611,869, 1997.
6. Jarema, C. P., "Paint Stripper Composition," U.S. Patent 5,468,415, 1995.
7. Koetzle, A. R., "High Temperature Flashpoint, Stable Cleaning Composition," U.S. Patent 5,498,805, 1996.
8. Larson, J. C., and Horton, G. L., "Cleaning Composition," U.S. Patent 5,230,821, 1993.
9. Rodzewich, E. A., "Metal Working Emulsion Cleaner," U.S. Patent 5,518,640, 1996.
10. Permsukarome, P., Chang, C., and Fogler, H. S., *Ind. Eng. Chem. Res*. **36,** 3960 (1997).
11. Beaudoin, S. P., Grant, C. S., and Carbonell, R. G., *Ind. Eng. Chem. Res.* **34,** 3307 (1995).
12. Beaudoin, S. P., Grant, C. S., and Carbonell, R. G., *Ind. Eng. Chem. Res.* **34,** 3318 (1995).
13. Kabin, J. A., Sáez, A. E., Grant, C. S., and Carbonell, R. G., *Ind. Eng. Chem. Res*. **35,** 4494 (1996).
14. Kabin, J. A., Sáez, A. E., Grant, C. S., and Carbonell, R. G., *Ind. Eng. Chem. Res*. **38,** 683 (1999).
15. Kabin, J. A., Tolstedt, S. L., Sáez, A. E., Grant, C. S., and Carbonell, R. G., *J. Colloid Interface Sci*. **206,** 102 (1998).
16. Yan, J., Sáez, A. E., and Grant, C. S., *AIChE J*. **43,** 251 (1997).
17. Grant, C. S., Perka, A. T., Thomas, W. D., and Caton, R., *AIChE J*. **42,** 1465 (1996).
18. Grant, C. S., Webb, G. E., and Jeon, Y. W., *AIChE J*. **42,** 861 (1996).
19. Littlejohn, F., Sáez, A. E., and Grant, C. S., *Ind. Eng. Chem. Res*. **37,** 2691 (1998).
20. Budavari, S., "The Merck Index," 11th ed., p. 1143, Merck, Rahway, NJ. 1989.
21. Adamczyk, Z., and Pomianowski, A., *Powder Technol*. **27,** 125 (1980).
22. Levich, B., *Acta Phicicochim. URSS* **17,** 257 (1942).
23. Geankoplis, C. J., "Transport Processes and Unit Operations," 2nd ed., Allyn and Bacon, Boston, 1983.
24. Mackay, D., and Shui, W. Y., *J. Chem. Eng. Data* **22,** 399 (1977).
25. Grimberg, S. J., Nagel, J., and Aitken, M. D., *Environ. Sci. Technol*. **29,** 1480 (1995).
26. May, W. E., and Wasik, S. P., *Anal. Chem.* **50,** 997 (1978).
27. Noggle, J. H., "Physical Chemistry," 2nd ed., Scott, Foresman, Glenview, 1989.
28. Dabros, T., Adamczyk, Z., and Czarnecki, J., *J. Colloid Interface Sci*. **62,** 529 (1977).
29. Adamczyk, Z., Dabros, T., and Czarnecki, J., *Acta Phys. Polonica A* **53,** 347 (1978).
30. Schenkel, J. H., and Kitchener, J. A., *Trans. Farady Soc*. **56,** 161 (1960).